

Perturbed phase-space dynamics of hard-disk fluids

Christina Forster^a, Robin Hirschl^{a,b}, Harald A. Posch^a,
William G. Hoover^c

^a*Institut für Experimentalphysik, Universität Wien, Boltzmannngasse 5, A-1090 Vienna, Austria*

^b*Institut für Materialphysik, Universität Wien, Boltzmannngasse 5, A-1090 Vienna, Austria*

^c*Department of Applied Science, University of California at Davis/Livermore and Methods Development Group, Lawrence Livermore National Laboratory, Livermore, California 94551-7808, USA*

Abstract

The Lyapunov spectrum describes the exponential growth, or decay, of infinitesimal phase-space perturbations. The perturbation associated with the maximum Lyapunov exponent is strongly localized in space, and only a small fraction of all particles contributes to the perturbation growth at any instant of time. This fraction converges to zero in the thermodynamic large-particle-number limit. For hard-disk and hard-sphere systems the perturbations belonging to the small positive and large negative exponents are coherently spread out and form orthogonal periodic structures in space, the “Lyapunov modes”. There are two types of mode polarizations, transverse and longitudinal. The transverse modes do not propagate, but the longitudinal modes do with a speed about one third of the sound speed. We characterize the symmetry and the degeneracy of the modes. In the thermodynamic limit the Lyapunov spectrum has a diverging slope near the intersection with the abscissa. No positive lower bound exists for the positive exponents. The mode amplitude scales with the inverse square root of the particle number as expected from the normalization of the perturbation vectors.

Key words: Hydrodynamic modes, Lyapunov spectrum, localized modes, fluid dynamics

PACS: 05.10.-a, 05.20.-y, 05.20.Jj, 05.45.Jn, 63.10.+a

Email addresses: tina@ap.univie.ac.at (Christina Forster),
Robin.Hirschl@univie.ac.at (Robin Hirschl), posch@ls.exp.univie.ac.at
(Harald A. Posch), hoover3011n1.gov (William G. Hoover).

1 Introduction

Recently, the concepts of dynamical systems theory and molecular dynamics simulations have been applied to the phase-space dynamics of models representing simple fluids and solids [1,2]. Due to the convex and dispersive nature of the atomic surfaces, the phase trajectory of such a system is highly Lyapunov unstable resulting in exponential growth, or decay, of small (infinitesimal) initial perturbations along specified directions in phase space. The respective rate constants, the Lyapunov exponents, are taken to be ordered by size with $\lambda_1 > 0$ representing the maximum exponent. The whole set, $\{\lambda_l, l = 1, \dots, 2dN\}$, is known as the Lyapunov spectrum, where d denotes the dimension of space, and N is the number of particles. For fluids in nonequilibrium steady states close links exist between the Lyapunov spectrum and various macroscopic dynamical properties – transport coefficients, irreversible entropy production, and the Second Law of thermodynamics [1–6]. This important result provides the motivation for us to examine also the spatial structure of the perturbations associated with the various exponents. Here we restrict ourselves to systems in thermodynamic equilibrium. Earlier accounts of our work have been published in Refs. [7–14].

Since the pioneering work of Bernal [15] with steel balls, and the seminal computer simulations of Alder and coworkers [16,17], hard ball systems are considered good models for the structure of “real” dense fluids. They serve as reference systems for highly-successful perturbation theories of liquids [18,19]. The dynamics, however, is rather different, and it is rewarding to study this difference, not only with the established machinery of correlation functions, but also from the viewpoint of dynamical systems theory. In this paper we discuss our results on the Lyapunov spectra and the space dependence of the associated perturbation vectors for two-dimensional hard disk systems in equilibrium. For comparison we also present related results for two-dimensional soft-disk fluids.

This work has three main objectives:

- 1) In Section 3 we demonstrate that the perturbation associated with the maximum Lyapunov exponent, λ_1 , is strongly localized in space: only a small fraction of all particles contributes actively to the growth of the perturbation norm at any instant of time. This localization persists in the thermodynamic limit, and, even more surprisingly, the fraction of simultaneously-contributing degrees of freedom converges to zero.
- 2) For small exponents close to the intersection with the abscissa the Lyapunov spectrum has a step-like appearance as is depicted in Fig. 1 for a two-dimensional 1024-disk fluid with particle density $\rho = 0.7$. The steps are caused by degenerate exponents, and the associated perturbations form coherent wave-like patterns in space with well-defined wave vectors and polariza-

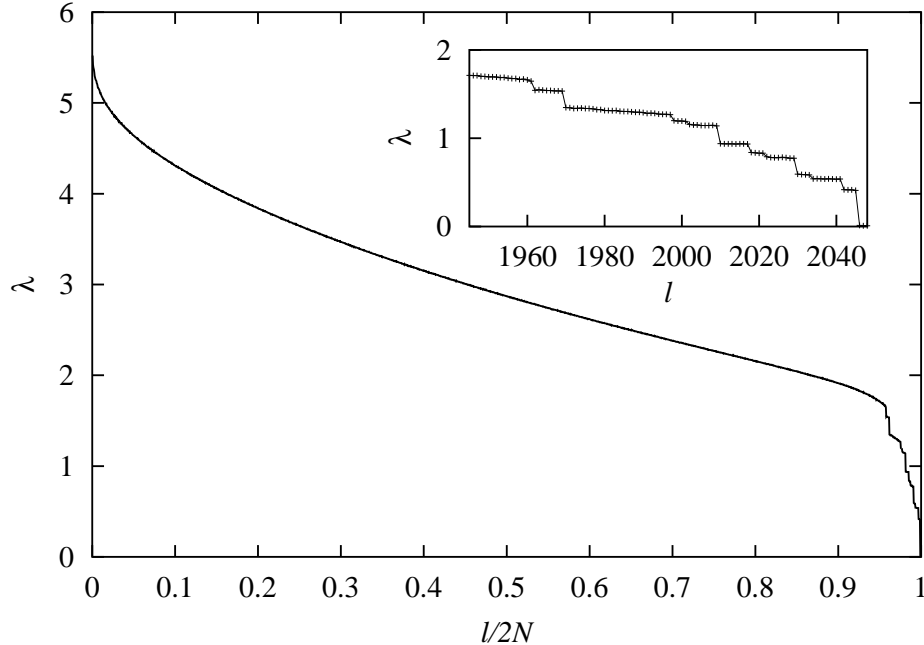


Fig. 1. Lyapunov spectrum of a 1024-disk system in a square simulation box with periodic boundaries. The density $\rho = 0.7$. A reduced index $l/2N$ is used on the abscissa. The steps are magnified in the inset. The non-normalized index, l , is used there. The spectrum is defined only for integer values of l .

tion. We refer to these patterns as “Lyapunov modes”. We have found them in hard-disk and hard-sphere systems in two and three dimensions [7–10], respectively, and in hard-dumbbell systems modelling fluids consisting of linear molecules [11–14]. In Section 4 we characterize the symmetry and polarization of these modes, where the emphasis is again on the thermodynamic limit for bulk systems: N and $V \rightarrow \infty$ such that $\rho = \text{const}$. V is the area of the box. We show that in this limit the Lyapunov spectrum has a vertical slope at the intersection point with the abscissa. No gap, or lower positive bound, exists for the positive exponents, and the smallest positive exponent converges linearly to zero with inverse system size.

3) How do the modes depend on the intermolecular potential? In Section 6 we discuss simulations of two-dimensional particle systems interacting with a continuous repulsive Weeks-Chandler-Anderson (WCA) potential. They reveal that the modes are extremely unstable and not easily observed. We relate this phenomenon to the strong fluctuations of the time-dependent local Lyapunov exponents.

Although many of the topics addressed here have been mentioned in our previous work [7–14], the simulation results and most of the analyses for square hard-disk systems are new. This applies, in particular, to the localization mea-

sure in Section 3, to the analysis of the perturbation vectors for the vanishing exponents in Section 4, to the discussions of the mode degeneracies and the construction of the Lyapunov spectrum in the thermodynamic limit in Section 5, and to the comments on mode stability in the same section. The tantalizing absence of stable collective modes for bulk Weeks-Chandler-Anderson fluids in Section 6 is a confirmation of our previous results on fluids interacting with another soft repulsive potential [10].

Since our discovery of the Lyapunov modes their theoretical foundation has been examined in some detail [20–26]. This work will be shortly summarized in the concluding Section 7. To facilitate the interpretation of our numerical results we outline our numerical methods for the computation of Lyapunov spectra for hard-disk systems [27,7] in the following section.

2 Lyapunov spectra and numerical procedure

The instantaneous state of a planar particle system is given by the $4N$ -dimensional phase-space vector $\mathbf{\Gamma} = \{\mathbf{q}_i, \mathbf{p}_i; i = 1, \dots, N\}$, where $\mathbf{q}_i = (x_i, y_i)$ and $\mathbf{p}_i = (p_{x,i}, p_{y,i})$ denote the position and linear momentum of particle i , respectively. An infinitesimal perturbation or offset vector $\delta\mathbf{\Gamma} = \{\delta\mathbf{q}_i, \delta\mathbf{p}_i; i = 1, \dots, N\}$ evolves according to motion equations obtained by linearizing the dynamical equations for $\mathbf{\Gamma}(t)$. For hard disks this amounts to a linearization of the collision map, which maps pre-collision into post-collision states in phase space [27]. There exist $4N$ orthonormal initial vectors $\{\delta\mathbf{\Gamma}_l(0); l = 1, \dots, 4N\}$ in tangent space, such that the Lyapunov exponents

$$\lambda_l = \lim_{t \rightarrow \infty} \frac{1}{t} \ln \frac{|\delta\mathbf{\Gamma}_l(t)|}{|\delta\mathbf{\Gamma}_l(0)|}, \quad l = 1, \dots, 4N, \quad (1)$$

exist and are independent of the initial state [29,30]. Geometrically, the Lyapunov spectrum describes the stretching and contraction along linearly-independent phase space directions of an infinitesimal hypersphere co-moving with the flow. According to the conjugate pairing rule [31–33] for symplectic systems, the exponents appear in pairs, and the pair sum vanishes, $\lambda_l + \lambda_{4N+1-l} = 0$. Thus, only the positive half of the spectrum $\{\lambda_{1 \leq l \leq 2N}\}$ needs to be calculated. Furthermore, six of the exponents, $\{\lambda_{2N-2 \leq l \leq 2N+3}\}$, vanish as a consequence of the conservation of energy, momentum, and center of mass, and of the non-exponential time evolution of a perturbation vector parallel to the phase flow.

For our numerical work we use a variant [27,7] of the classical algorithm by Benettin *et al.* and Shimada and Nagashima [34,35], where the reference trajectory and the orthonormal set of perturbation vectors are simultaneously

evolved in time. The latter are periodically re-orthonormalized with a Gram-Schmidt (GS) procedure after consecutive time intervals Δt_{GS} , which were chosen according to $\Delta t_{GS} \simeq \tau_2/5$. Here, $\tau_2 = (\beta m)^{1/2}/(2\pi^{1/2}\rho\sigma)$ is the collision time per particle, $\beta = (k_B T)^{-1}$, T is the temperature, k_B is Boltzmann's constant, and σ is the disk diameter. The Lyapunov exponents are determined from the time-averaged renormalization factors.

Fig. 1 shows the positive branch of the Lyapunov spectrum for a 1024-disk system in a square simulation box with periodic boundaries. If not stated otherwise, reduced units are used for which the particle diameter σ , the particle mass m , and the kinetic energy per particle, $K/N \equiv k_B T$, are unity. Thus, the unit of time is $t^* = (m\sigma^2 N/K)^{1/2}$, and the Lyapunov exponents are given in units of $1/t^*$. The simulation box has lengths L_x and L_y . In all our examples the density $\rho \equiv N/(L_x L_y)$ is 0.7, which is slightly smaller than the fluid-to-solid phase transition density.

3 Localized mode for the maximum exponent

The maximum exponent is dominated by the fastest dynamical events. There is strong numerical evidence that the thermodynamic limit $\{N, V \rightarrow \infty, N/V \text{ constant}\}$ for λ_1 and, hence, for the whole spectrum exists [27,13]. The associated perturbation is strongly localized in space [28,12,13]. This is demonstrated by projecting the perturbation vector $\delta\mathbf{\Gamma}_1$ onto the four-dimensional subspaces spanned by the components belonging to the individual particles. The squared norm of this projection, $|\delta\mathbf{q}_i|^2 + |\delta\mathbf{p}_i|^2$, indicates how active a particle i is engaged in the growth process characterized by λ_1 [13,12]. In Fig. 2 it is plotted for a 1024-disk system at the particle positions (x_i, y_i) , where the ensuing surface is interpolated over a periodic grid covering the simulation box. The figure refers to an instantaneous configuration of a well-relaxed system. The fastest expansion activity is clearly confined to a few very active zones.

To understand this localization we note that the offset-vector dynamics is governed by *linear* equations and that a perturbation component has only a fair chance of further growth if its value was already above average before a collision. Each global renormalization step tends to reduce the (already small) components of the other non-colliding particles even further. There is a competition for growth which favors the particles with the largest perturbation components. The few active zones move diffusively in space and perform occasional jumps.

The localization persists in the thermodynamic limit. To show this [13] we order all squared components $[\delta\mathbf{\Gamma}_l]_j^2$; $j = 1, \dots, 4N$ of a perturbation vector $\delta\mathbf{\Gamma}_l$ according to size. By adding them up, starting with the largest, we determine

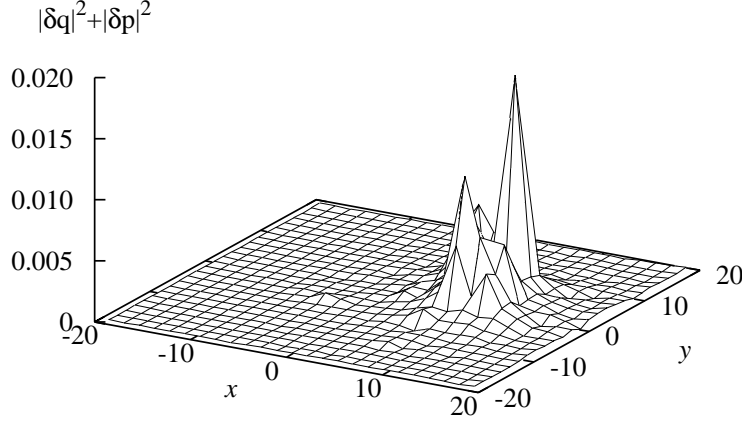


Fig. 2. Squared norm of the individual particle perturbations, $|\delta\mathbf{q}_i|^2 + |\delta\mathbf{p}_i|^2$, for the offset vector associated with λ_1 , plotted at the positions $\mathbf{q}_i = (x_i, y_i)$ of the particles. The ensuing surface is linearly interpolated over a periodic grid covering the simulation box. The system consists of 1024 hard disks in a square box with periodic boundaries, at a density $\rho = 0.7$, and a temperature $T = K/N = 1$.

the smallest number of terms, n , which are required for the sum to exceed a threshold Θ . $C_{l,\Theta} \equiv n/4N$ is a *relative* measure for the number of components contributing to λ_l :

$$\Theta \leq \left\langle \sum_{s=1}^{4NC_{l,\Theta}} [\delta\mathbf{\Gamma}_l]_s^2 \right\rangle, \quad [\delta\mathbf{\Gamma}_l]_i^2 \geq [\delta\mathbf{\Gamma}_l]_j^2 \text{ for } i < j. \quad (2)$$

The angular brackets denote a time average. From the normalization of the perturbation vectors it follows that $C_{l,1} = 1$. In Fig. 3 the localization measure, for $l = 1$ and for a threshold $\Theta = 0.98$, is shown as a function of the particle number N . It obeys a power law with a negative power, and converges to zero for $N \rightarrow \infty$. The ratio of tangent-vector components (and, hence, of particles) contributing significantly to the maximum Lyapunov exponent vanishes in that limit. A power-law dependence for the localization measure is a very general result, although the parameters are sensitive to the interaction potential [9,36].

If the localization measure is plotted for all positive exponents with index $1 \leq l \leq 2N$ as depicted in Fig. 4, one observes a fast increase for small l , where the full dot indicates the result for $l = 1$. This is an indication that the localization does not persist for large l and that the perturbation growth starts to involve more and more particle components. The inset shows the interesting regime for which modes have been observed.

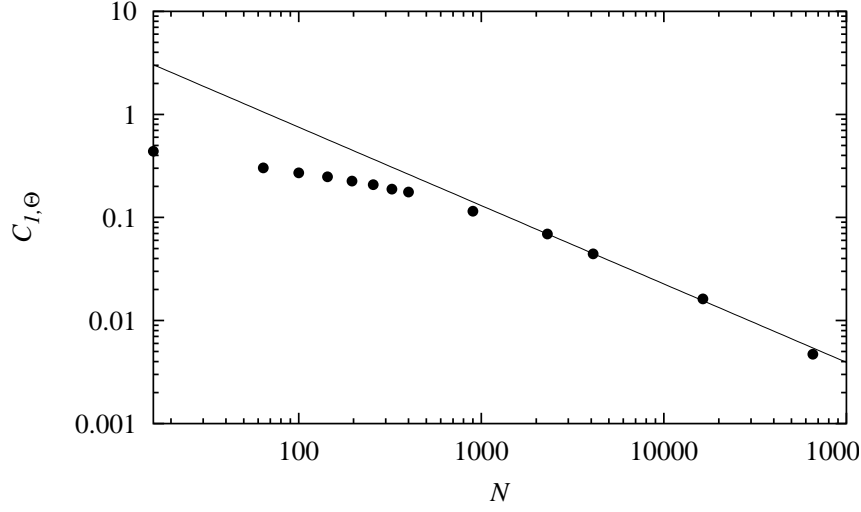


Fig. 3. Particle-number dependence of the localization measure for the perturbation belonging to the maximum exponent, $C_{l,\Theta}$. The threshold Θ is 0.98. The line represents a power law, $25N^{-0.76}$.

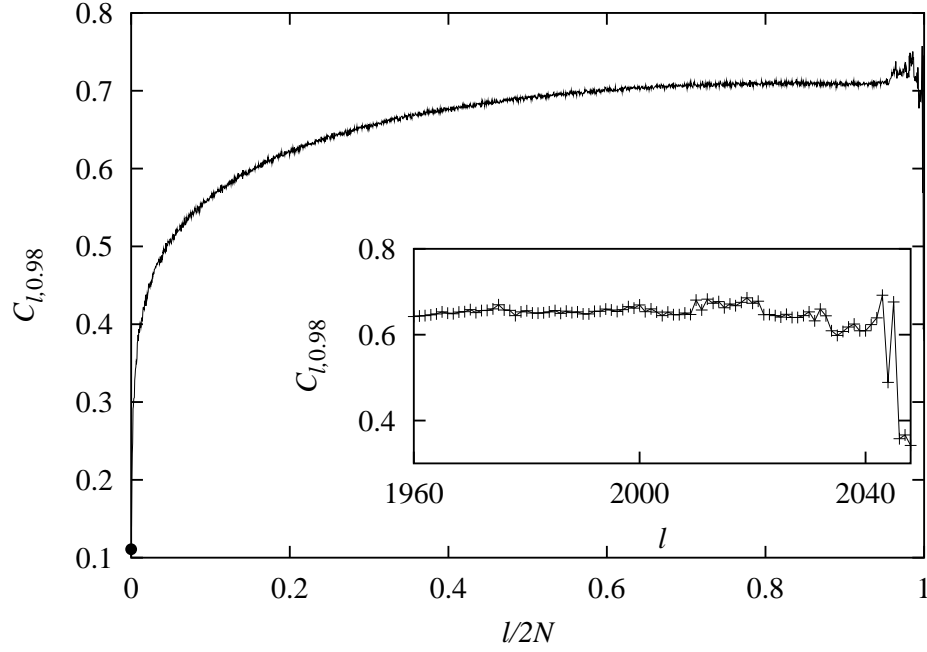


Fig. 4. Dependence of the localization measure $C_{l,\Theta=0.98}$ on the reduced Lyapunov index $l/2N$. The system consists of $N = 1024$ particles, and the density ρ is 0.7. The inset provides an enlargement of the mode regime. Here, the Lyapunov index l is not normalized.

4 Perturbation vectors for the six vanishing exponents

To be explicit, we arrange the components of the $4N$ -dimensional state vector according to

$$\mathbf{\Gamma} = (x_1, y_1, \dots, x_N, y_N; p_{x,1}, p_{y,1}, \dots, p_{x,N}, p_{y,N}) . \quad (3)$$

During the streaming motion in between instantaneous elastic collisions no forces act between the particles, and a normalized vector parallel to the phase flow $\dot{\mathbf{\Gamma}}$ becomes

$$\mathbf{e}_1 = (1/\sqrt{2K})(p_{x,1}, p_{y,1}, \dots, p_{x,N}, p_{y,N}; 0, 0, \dots, 0, 0) . \quad (4)$$

A perturbation vector parallel to \mathbf{e}_1 does not grow exponentially with time and contributes one vanishing exponent to the full spectrum [5].

The motion in the extended $4N$ -dimensional phase space is constrained to hypersurfaces generated by center-of-mass conservation, $(\sum_{j=1}^N x_{j,1} = \text{const}, \sum_{j=1}^N y_{j,1} = \text{const})$, by momentum conservation, $(\sum_{j=1}^N p_{x,j} = 0, \sum_{j=1}^N p_{y,j} = 0)$, and by the conservation of energy $(\sum_{j=1}^N (p_{x,j}^2 + p_{y,j}^2)/2 = K)$. All respective vectors orthogonal to these surfaces also denote directions of non-exponential phase-space expansion or compression:

$$\mathbf{e}_2 = (1/\sqrt{N})(1, 0, \dots, 1, 0; 0, 0, \dots, 0, 0) \quad (5)$$

$$\mathbf{e}_3 = (1/\sqrt{N})(0, 1, \dots, 0, 1; 0, 0, \dots, 0, 0) \quad (6)$$

$$\mathbf{e}_4 = (1/\sqrt{N})(0, 0, \dots, 0, 0; 1, 0, \dots, 1, 0) \quad (7)$$

$$\mathbf{e}_5 = (1/\sqrt{N})(0, 0, \dots, 0, 0; 0, 1, \dots, 0, 1) \quad (8)$$

$$\mathbf{e}_6 = (1/\sqrt{2K})(0, 0, \dots, 0, 0; p_{x,1}, p_{y,1}, \dots, p_{x,N}, p_{y,N}) . \quad (9)$$

The vectors \mathbf{e}_1 to \mathbf{e}_6 are orthonormal and form the basis of an invariant subspace, the central manifold, which contains also the six perturbation vectors $\{\delta\mathbf{\Gamma}_l, 2N - 2 \leq l \leq 2N + 3\}$ responsible for the vanishing exponents. An expansion in the natural basis gives

$$\delta\mathbf{\Gamma}_l = \sum_{i=1}^6 \alpha_{l,i} \mathbf{e}_i, \quad l = 2N - 2, \dots, 2N + 3 . \quad (10)$$

The matrix of the projection cosines, $\alpha_{l,i} = (\delta\mathbf{\Gamma}_l \cdot \mathbf{e}_i)$, obeys the normalization conditions

$$\sum_{i=1}^6 (\alpha_{l,i})^2 = 1 \quad , \quad \sum_{l=2N-2}^{2N+3} (\alpha_{l,i})^2 = 1 ,$$

Table 1

Projection cosines of the perturbation vectors in the central manifold onto the natural basis vectors for a well-relaxed configuration of a 400-disk fluid with density $\rho = 0.7$ and a total kinetic energy $K = N$.

l	$\alpha_{l,1}$	$\alpha_{l,2}$	$\alpha_{l,3}$	$\alpha_{l,4}$	$\alpha_{l,5}$	$\alpha_{l,6}$
398	0.431	0.297	-0.852	0	0	0
399	0.549	-0.836	-0.013	0	0	0
400	-0.716	-0.462	-0.523	0	0	0
401	0	0	0	-0.138	-0.607	-0.783
402	0	0	0	-0.620	0.669	-0.409
403	0	0	0	-0.772	-0.429	0.469

if the total momentum vanishes and if $K = N$ as is always the case in our simulations. As an example we list such a matrix in Table 1 for a 400-disk fluid. We note that these numbers are the asymptotic values for a well-relaxed system and do not change with time. They always appear in block-diagonal form, but other than that they depend on the initial conditions for the simulation. The block-diagonal structure indicates that the subspaces $\mathcal{C}^+ = \text{span}\{\mathbf{e}_1, \mathbf{e}_2, \mathbf{e}_3\}$ and $\mathcal{C}^- = \text{span}\{\mathbf{e}_4, \mathbf{e}_5, \mathbf{e}_6\}$ are asymptotically ordered by the Gram-Schmidt procedure due to *linear* perturbation growth/decay during the streaming motion between successive collisions. This may be seen explicitly from the linear motion equations for intercollisional streaming and the linearized collision map. For example, perturbations $\delta\Gamma$, parallel to \mathbf{e}_1 , \mathbf{e}_2 , or \mathbf{e}_3 at $t = 0$ immediately after a collision, will continue to be so at a later time $t > 0$. However, perturbations $\delta\Gamma$ parallel to \mathbf{e}_4 , \mathbf{e}_5 , and \mathbf{e}_6 at time zero, evolve according to $\mathbf{e}_2t + \mathbf{e}_4$, $\mathbf{e}_3t + \mathbf{e}_5$, and $\mathbf{e}_1t + \mathbf{e}_6$, respectively, for $t > 0$ previous to the next collision.

5 Lyapunov modes

5.1 Classification of the modes

Next, we study the non-localized perturbations associated with the small positive exponents. The simulation box is a square with $L_x = L_y = L$. The inset in Fig. 1 gives an enlargement of the step-like structure for a 1024-disk spectrum.

The first step consists of four degenerate exponents, for which $l = 2045, 2044, 2043$ and 2042 . On the left-hand side of Fig. 5 we plot the positional perturbation components, δx_i and δy_i , of the particles at their positions (x_i, y_i) in the simulation box, where the surfaces have been linearly interpolated on a periodic grid covering the simulation box. One finds periodic patterns like sines and cosines, with a phase shift of $\pi/2$ between them. The wave vectors for δx and δy are orthogonal to the y and x axes, respectively, and we refer to these

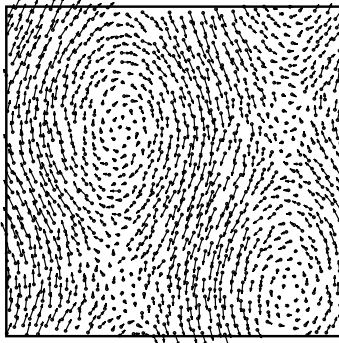
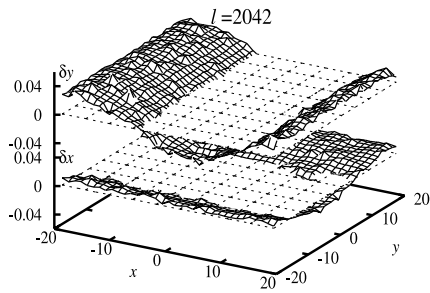
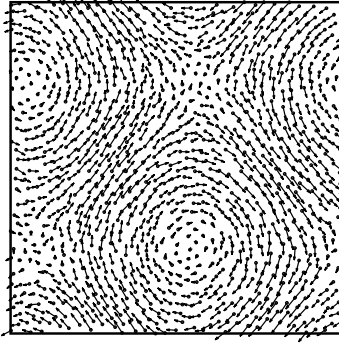
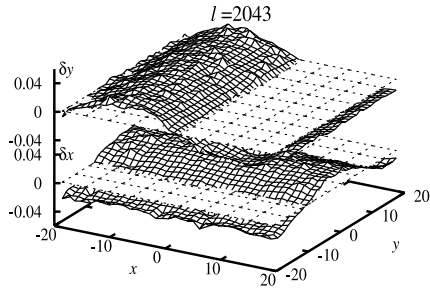
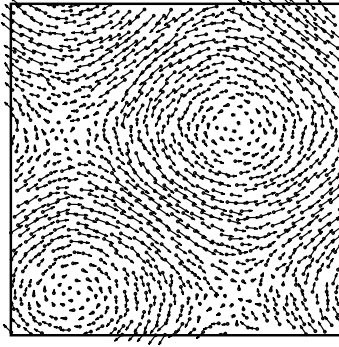
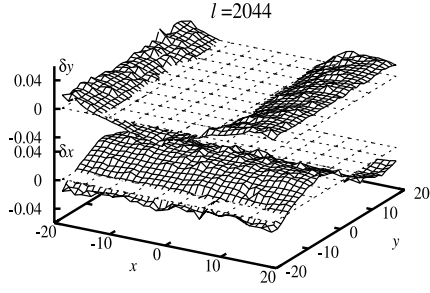
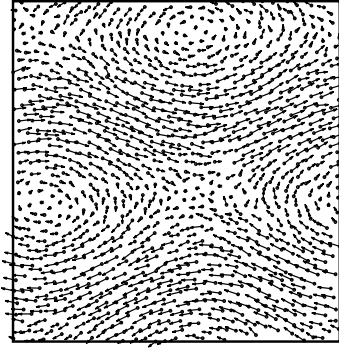
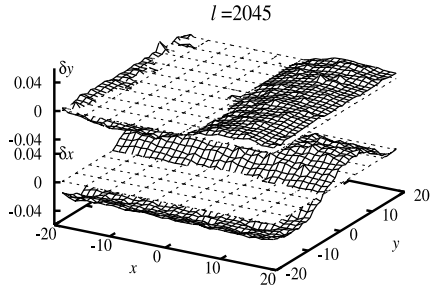


Fig. 5. Transverse modes with the smallest-possible wave number for $l = 2045$, 2044, 2043 and 2042. The fluid consists of 1024 disks with a density $\rho = 0.7$. See the main text for details.

modes as *transverse*. Their wave number, $k \equiv |\mathbf{k}|$, is the smallest consistent with the periodic boundaries, $k_l = 2\pi/L$ for $2042 \leq l \leq 2044$. The same transverse modes, in another representation, are shown on the right-hand side of Fig. 5, where the particle perturbations $(\delta x_i, \delta y_i)$ for all particles i are plotted as small arrows at the respective particle positions. Transverse modes do not propagate.

The next-larger exponents responsible for the second step in the inset of Fig. 1 have multiplicity eight, $2034 \leq l \leq 2041$. Their modes are called *longitudinal*, since the perturbations δx and δy are parallel to their respective wave vectors with wave number $2\pi/L$. Longitudinal modes are propagating, with a phase velocity roughly equal to one third of the sound speed [8].

Continuing up the steps, one encounters transverse modes for $2030 \leq l \leq 2033$ with multiplicity 4 and wave vectors pointing along the diagonals of the simulation box, $k = 2\sqrt{2}\pi/L$, followed by longitudinal modes for $2030 \leq l \leq 2033$, with multiplicity 8 and wave vectors also along the diagonals, $k = 2\sqrt{2}\pi/L$, and so on. In the general case of a rectangular simulation box, all modes look like waves with n_x nodes in x direction and n_y nodes in y direction, such that

$$k = 2\pi \sqrt{\left(\frac{n_x}{L_x}\right)^2 + \left(\frac{n_y}{L_y}\right)^2}. \quad (11)$$

The case $n_x = n_y = 0$ corresponds to perturbation vectors in the central manifold and has been treated in the previous section. For all positive exponents the momentum perturbations δp_x and δp_y are strictly parallel to the respective positional perturbations δx and δy , and are therefore not included in Fig. 5.

All modes may be classified either as transverse or longitudinal, where the dependence of the Lyapunov exponents on k differs for each class. This is shown in Fig. 6, in which all small exponents, plotted as a function of k , lie on two curves, one for the transverse (T) and one for the longitudinal (L) modes. To second order in k , these “dispersion relations” may be approximated by

$$\lambda_T = 2.48(3)k + 0.23(7)k^2 + \mathcal{O}(k^3) \quad (12)$$

$$\lambda_L = 3.13(7)k + 1.2(2)k^2 + \mathcal{O}(k^3). \quad (13)$$

The standard deviations affect the last digit of the fit parameters and are given in brackets. These second-order approximations are indicated as dashed lines in Fig. 6. It has been argued by Mareschal and McNamara [23] that the k^2 term is negligible. However, the data, in particular the longitudinal exponents, are better represented if this term is kept, although it is unessential for the discussion below.

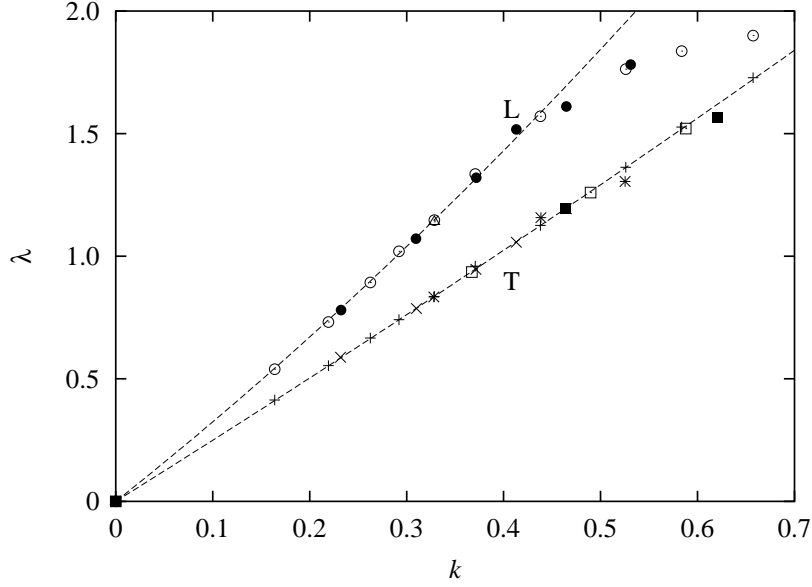


Fig. 6. Dependence of the small positive Lyapunov exponents on the wave number k for various systems containing between 100 and 1024 particles. L refers to longitudinal, and T to transverse modes. The density of the hard-disk fluid is 0.7, the kinetic energy per particle, K/N , is unity.

5.2 Mode degeneracy

The degeneracy of the Lyapunov exponents is a consequence of the square symmetry of the periodic simulation box and the phase shift of $\pi/2$ between sine and cosine-like patterns, allowing for different *orthogonal* perturbations with the same k . For the non-propagating *transverse* modes the sense of direction is not needed. It suffices to consider all wave vectors in a half plane of the reciprocal lattice, as on the left-hand side of Fig. 7. The full and open circles refer to sine and cosine-like waves, respectively, which have to be counted separately. Degenerate modes belong to all lattice points on a circle with a specified radius k . Their multiplicity is denoted by M_k . For the propagating *longitudinal* modes the full reciprocal lattice plane is needed as on the right-hand side of Fig. 7. As a consequence, the degeneracy of the longitudinal modes is always twice that of the transverse modes for a given k . With the circles in Fig. 7 we select degenerate modes with $k = 2\sqrt{5}\pi/L$ as examples. The transverse modes have multiplicity 8 and appear for $l = 2010, \dots, 2017$ in the 1024-disk spectrum of Fig 8. The longitudinal modes have multiplicity 16 and are indexed by $l = 1978, \dots, 1993$. Of course, the relative position of a degenerate group of exponents in the spectrum is determined by the dispersion relations given above.

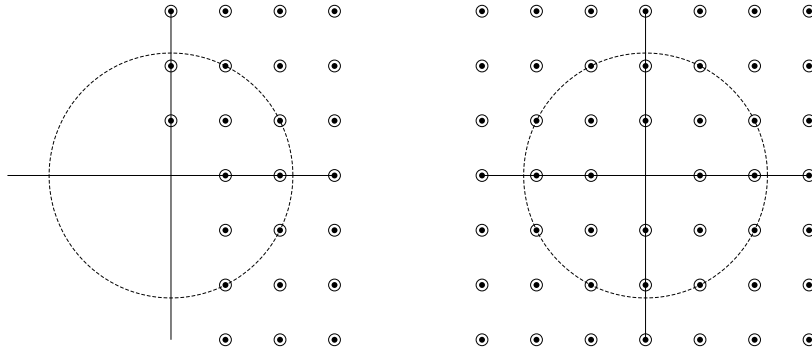


Fig. 7. Reciprocal lattice with point spacing equal to $2\pi/L$, for sine-like patterns (open circles) and cosine-like patterns (dots). Transverse modes do not require a sense of direction, and only one half plane is needed (left), whereas for longitudinal modes the full reciprocal lattice is required (right). The circle connects allowed wave vectors with $k = 2\sqrt{5}\pi/L$.

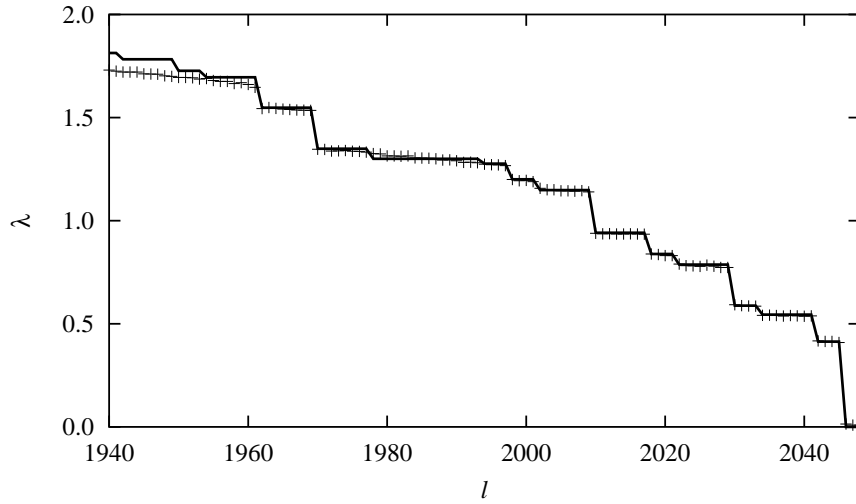


Fig. 8. Small positive Lyapunov exponents for a 1024-disk system: the crosses denote simulation results, the smooth curve indicates the reconstruction to second order in k as described in the main text.

5.3 Mode amplitudes and stability of transverse modes

Each mode with index l is viewed here as a four-dimensional field on the periodic domain of the simulation box, and will be denoted by ¹,

$$\mathcal{P}_l(x, y) = \{\delta x(x, y), \delta y(x, y), \delta p_x(x, y), \delta p_y(x, y)\}_l. \quad (14)$$

¹ Sometimes it is advantageous to label the fields, \mathcal{P}_l , not by l but by the wave-vector norm k and an integer m distinguishing different modes within a degenerate group, $1 \leq m \leq M_k$

Its norm,

$$|\mathcal{P}_l(x, y)| = [(\delta x)^2 + (\delta y)^2 + (\delta p_x)^2 + (\delta p_y)^2]_l^{1/2}, \quad (15)$$

is also a periodic function on the domain with amplitude P_0^l . Since $\delta\Gamma_l$ is normalized, it follows that

$$\int_0^L \int_0^L |\mathcal{P}_l(x, y)|^2 dx dy = 1. \quad (16)$$

As an example we consider again the transverse modes for $l = 2N - 3$ belonging to the first step in the spectrum. For $N = 1024$ such a mode is shown at the top of Fig. 5. For any N it has the simple structure

$$\mathcal{P}_{2N-3}(x, y) = \{(\delta x)_0 \sin(ky + \phi_y), (\delta y)_0 \sin(kx + \phi_x), \\ (\delta p_x)_0 \sin(ky + \phi_y), (\delta p_y)_0 \sin(kx + \phi_x)\}_{2N-3}, \quad (17)$$

where $k = 2\pi/L$. The phases ϕ_x and ϕ_y are equal for this particular example, but in a more general case they may differ by π .

The mode amplitude may be expressed in terms of the component amplitudes according to

$$P_0^{2N-3} = [(\delta x)_0^2 + (\delta y)_0^2 + (\delta p_x)_0^2 + (\delta p_y)_0^2]^{1/2}. \quad (18)$$

The box-size and, hence, the particle-number dependence of this quantity follows immediately from the normalization condition Eq. (16):

$$P_0^{2N-3} = \left(\frac{2}{N}\right)^{1/2}. \quad (19)$$

The amplitude vanishes in the thermodynamic limit [20]. In Fig. 9 the dependence of P_0^{2N-3} on $\sqrt{N} = L$ is shown. The dots are numerical results, where the mode amplitude is obtained from fits of the components of Eq. (17) to the data. The smooth line is the result predicted by Eq. (19). Similar results are obtained for the other modes. The good agreement between theory and experiment is an indication for the remarkable stability of the modes.

It should be pointed out that only the mode amplitude derived from the vector norm, Eq. (15), displays the correct system-size dependence. The amplitudes of the vector components do not. Even $(\delta x)_0$ and $(\delta y)_0$ do not agree in general. The amplitudes of the field components depend on the initial conditions of the simulation, but P_0^l does not.

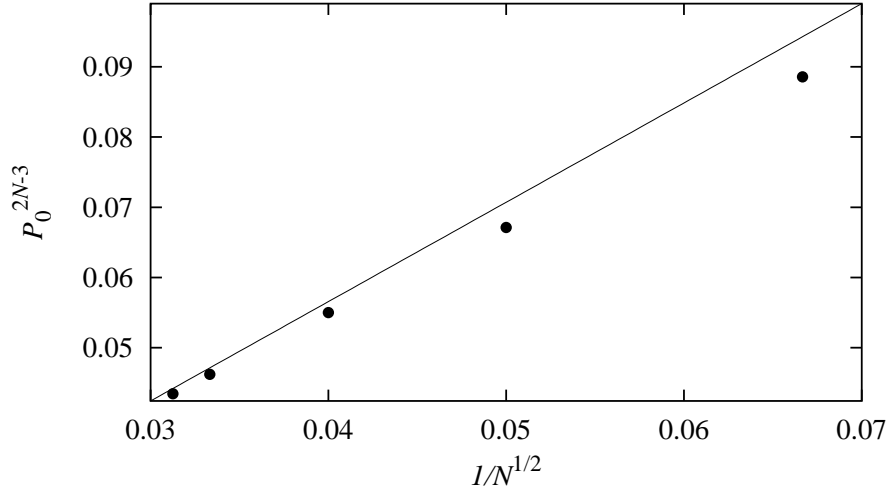


Fig. 9. The dots indicate the $1/\sqrt{N}$ dependence of the transverse-mode amplitude P_0^{2N-3} corresponding to the first nonvanishing exponent λ_{2N-3} . The smooth line is the prediction of Eq. (19).

5.4 Spectrum reconstruction near the thermodynamic limit

If the dispersion relations are known for a fluid of a given density, the rules outlined above allow a reconstruction of the most-interesting spectral range for small positive exponents. If the second-order approximations of Eqs. (12) and (13) are used, the reconstructed spectrum for the 1024-disk system is indicated in Fig. 8 by a smooth line. As expected, it agrees very well with the direct simulation results for $l > 1962$ corresponding to small k . Since Eqs. (12) and (13) apply to the $k \rightarrow 0$ limit, very large systems may be studied which are not accessible by direct simulation, now and in the foreseeable future. In Fig. 10 a reconstructed spectrum for a fluid containing 40,000 disks with a density 0.7 is shown, which may be considered to be close to the thermodynamic limit. Only a very small part of the spectrum is actually shown, for which k does not exceed 0.3. We may fit a power law to these spectral points,

$$\lambda_l = \alpha \left[1 - \frac{l}{2N} \right]^\beta, \quad 0.99 < \frac{l}{2N} < 1, \quad (20)$$

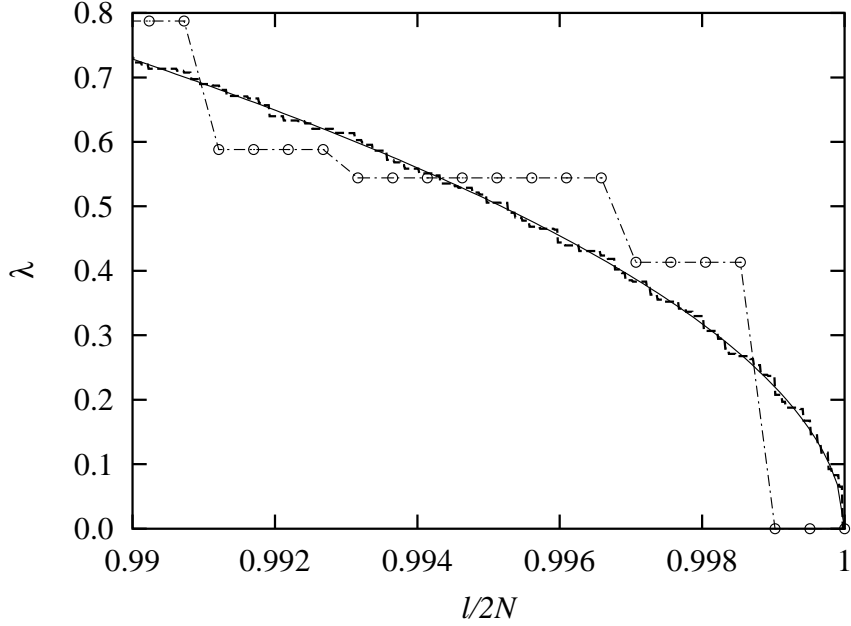


Fig. 10. Part of a reconstructed Lyapunov spectrum for a fluid of density 0.7, consisting of 40,000 disks, is shown by the dashed line. The smooth line is a fit of these points to a power law, Eq. (20). For comparison, the spectrum for 1024 disks is also shown by the points. On the abscissa a normalized index $l/2N$ is used.

with $\alpha = 7.81 \pm 0.04$ and $\beta = 0.52 \pm 0.01$.² The slope of the spectrum near the intersection with the abscissa,

$$\lim_{l/2N \rightarrow 1} \frac{d\lambda_l}{d(l/2N)} \sim \lim_{l/2N \rightarrow 1} \left[1 - \frac{l}{2N} \right]^{-0.48} \quad (21)$$

diverges for $l/2N \rightarrow 1$. Since the small positive exponents approach zero linearly with k as expressed by the dispersion relations above, no gap appears in the spectrum. No lower positive bound exists for the positive Lyapunov exponents. An analogous statement for the negative exponents of the spectrum holds due to the conjugate pairing symmetry of the spectrum.

We have also extended these considerations to quasi-one-dimensional systems [36,37], for which the aspect ratio of the simulation box, $A \equiv L_y/L_x$, converges to zero in the large-particle limit. This is achieved by fixing the box size L_y in y direction, typically a few particle diameters, and letting L_x become large such that the particle density remains constant. The Lyapunov modes are more obvious in this case, since the reciprocal lattice consists of equidistant points on

² We note that for a simple model of a two-dimensional solid the number of vibrational modes dl between wave numbers k and $k+dk$ is proportional to k . Integrating this relation and assuming linear dispersion relations for the Lyapunov exponents we obtain $\lambda \sim l^{1/2}$ [1]. This power closely agrees with our value for β .

the abscissa, allowing only multiplicity two for the transverse modes, and four for the longitudinal. The limiting spectral slope near the intersection with the abscissa remains finite [36]. Very recently, Taniguchi and Morriss [38] have also studied other than periodic boundary conditions for very narrow quasi-one-dimensional systems, for which the particles cannot cross. Equivalent modes are observed.

So far we have concentrated on the positive branch of the Lyapunov spectrum, for which the components of the momentum perturbations are parallel to the respective perturbation components for the positions. This is a consequence of the linearity of the motion equations in tangent space and the positivity of the exponents. For the negative branch of the spectrum the momentum components are antiparallel to the position components of the perturbations. All our statements concerning the multiplicity and polarization of the modes carry over also to this case.

6 A puzzle provided by the soft potential

What happens if the interparticle potential is soft? In Refs. [10,9] a comparison was made between soft and hard-disk systems and, surprisingly, no modes could be clearly identified. Here we extend this work by considering two-dimensional soft fluids with a Weeks-Chandler-Anderson (WCA) interaction potential,

$$\phi(r) = \begin{cases} 4\epsilon[(\sigma/r)^{12} - (\sigma/r)^6] + \epsilon, & r < 2^{1/6}\sigma \\ 0, & r \geq 2^{1/6}\sigma. \end{cases} \quad (22)$$

We use units for which the particle mass m , the particle diameter σ , and the energy parameter ϵ are unity. Furthermore, we consider a thermodynamic state with a total energy per particle, E/N , also equal to unity. Since there is a potential energy in this case, a comparison between soft and hard disks is done for equal temperatures $T \equiv K/N$ (and not for equal energy), where Boltzmann's constant is also set to unity. All hard-disk Lyapunov exponents quoted in this section are therefore rescaled by a factor $\sqrt{(K/N)_{WCA}/(K/N)_{HD}}$, where K is the total kinetic energy. Since the soft-potential spectra are computationally more expensive, we restrict our examples to $N \leq 100$.

The spectra for the soft- and hard-disk fluids in Fig. 11 are surprisingly different, both in shape and in absolute value. Most conspicuously, no steps are observed in the WCA case, whereas for hard disks at least the lowest step is well developed. This comparison provides us with the following facts [9,36]:

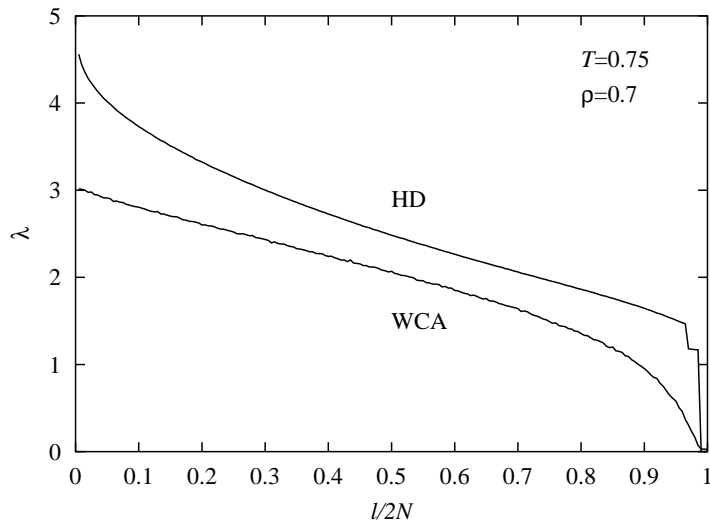


Fig. 11. Lyapunov spectra for 100 soft (WCA) and hard (HD) disks at a density $\rho = 0.7$ and a temperature $T = 0.75$. The simulation box is a square with periodic boundary conditions

- 1) The overall shape of the WCA spectrum may be approximated by a power law similar to Eq. (20), but with a power of the order of 0.4, (which depends slightly on the fitting range). A similar behavior has been found for three-dimensional WCA fluids, and has been interpreted there in terms of a simple Debye model for the distribution of vibrational frequencies in solids, anticipating the Lyapunov modes. For details we refer to Ref. [1], although the systems there are too small for a meaningful comparison with the hard-disk fluids.
- 2) If the WCA potential is made progressively steeper, its spectrum converges towards that of hard disks, and the step structure starts to re-appear [36]. This convergence, however, is slow, in particular for the largest exponent λ_1 .
- 3) The perturbation vector associated with λ_1 is also localized for soft disks, and this localization persists in the thermodynamic limit. An instantaneous snapshot of such a perturbation for 100 WCA particles looks very similar to Fig. 2. Also the localization measure $C_{1,\theta}$ introduced in Section 3 is found to obey a power law with a negative power of N [37]: $C_{1,\theta=0.92} = 0.31N^{-0.10}$ for a WCA fluid with $\rho = 0.7$ and $T = 0.75$. Only a few particles, localized in space, provide the main contributions to the perturbation vector $\delta\mathbf{T}_1$. However, there is a very sensitive dependence of the details on the interparticle potential.
- 4) As we suspected from the absence of a step structure, no Lyapunov modes could be reliably identified, either visually or by Fourier-transformation techniques. Although it is possible to see patterns resembling transverse modes for the smallest exponent, these patterns are transient and too unstable to survive time averaging [10]. This observation is consistent with large fluctuations of the local time-dependent exponents λ'_l , from which the Lyapunov exponents

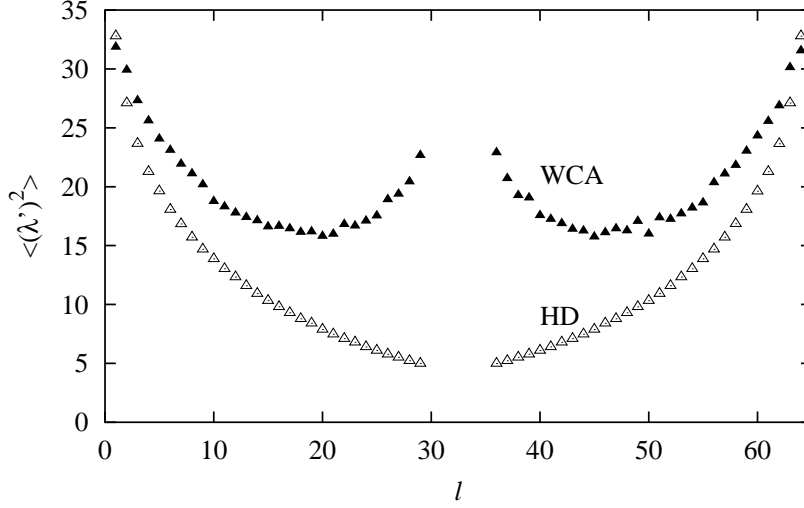


Fig. 12. Second moments of the time-dependent local exponents for a planar 16-particle system. The labels WCA and HD refer to the Weeks-Chandler-Anderson and hard disk models, respectively. The re-orthonormalization time $\Delta t_{GS} = 0.075$, the temperature $T = 0.75$, and the density $\rho = 0.7$.

are obtained by time averaging:

$$\lambda_l = \lim_{\tau \rightarrow \infty} \frac{1}{\tau} \int_0^\tau \lambda'_l(\Gamma(t)) dt. \quad (23)$$

$\lambda'_l(\Gamma)$ depends on the state $\Gamma(t)$ the system occupies in phase space at time t and, of course, on a long-enough part of the trajectory terminating at this point. They may be estimated from

$$\lambda'_l(\Gamma(t)) = \frac{1}{\Delta t_{GS}} \ln \frac{|\delta \Gamma_l(\Gamma(t + \Delta t_{GS}))|}{|\delta \Gamma_l(\Gamma(t))|}, \quad (24)$$

where t and $t + \Delta t_{GS}$ refer to times immediately after consecutive Gram-Schmidt re-orthonormalization steps. In Fig. 12 the second moments of these quantities, $\{\langle \lambda_l'^2 \rangle\}$, $l = 1, \dots, 4N$, time averaged along the phase trajectory, are shown for 16-particle WCA and hard-disk systems, where a re-orthonormalization interval 0.075 is used³. $l = 1$ refers to the maximum, and $l = 64$ to the most-negative exponent. The points for $30 \leq l \leq 35$ correspond to the 6 vanishing exponents and are not shown. We infer from this figure that for the

³ The computation of the second moments $\langle \lambda_l'^2 \rangle$ for hard disks requires some care. For small re-orthonormalization intervals Δt_{GS} , the variance $\langle \lambda_l'^2 \rangle - \langle \lambda_l' \rangle^2$ varies with $1/\Delta t_{GS}$ and diverges for $\Delta t_{GS} \rightarrow 0$, but the shape of the fluctuation spectrum is hardly affected by the size of Δt_{GS} .

soft WCA particles the fluctuations of the local exponents become very large for the Lyapunov exponents describing relatively-weak instabilities with near-zero growth rates, $l \rightarrow 2N$. For the hard disk system, however, the relative significance of the fluctuations becomes minimal in this regime.

7 Outlook

Soon after the discovery of the Lyapunov modes, Eckmann and Gat [20] were the first to provide theoretical arguments for the existence of hydrodynamic-like Lyapunov modes. They were derived from the translation invariance of the systems, and were based on an evolution matrix in tangent space modeled as a product of independent random matrices. No accompanying real space dynamics exists for this model. Most recently, this theory has been improved and made more realistic by Eckmann and Zabey [21]. In another approach, McNamara and Mareschal [22] isolate the six hydrodynamic fields related to the invariants of the binary particle collisions and the vanishing exponents, and use a generalized Enskog theory to derive hydrodynamic evolution equations for these fields. Their solutions are the Lyapunov modes. In a more detailed extension of this work a generalized probability distribution is used, which, in addition to the position and momentum, also involves the respective tangent-space perturbations. From the Boltzman equation for this generalized distribution the hydrodynamic evolution equations for the perturbation fields are derived [23]. However, the quantitative aspects of this theory are restricted to small densities. A related approach was taken by de Wijn and van Beijeren [24]. Finally, Taniguchi, Dettmann, and Morriss have approached the problem using periodic orbit theory [25] and master equations [26].

We have mentioned in Section 6 that for small positive exponents the Lyapunov spectrum is well described by a power-law close to the thermodynamic limit, and that no positive lower bound exists in this case. This has raised questions about the numerical accuracy and convergence of our results. With respect to the former, we have verified that quadruple precision (128 bits) arithmetic gives the same results as the usual double-precision arithmetic. To answer the question of convergence, we have perturbed an already well-oriented set of orthonormal tangent vectors for a well-relaxed system and have ascertained that the unperturbed and perturbed sets of vectors become identical again after a certain transient time. The relaxation time the tangent vectors require to reach their proper orientations has been studied in Ref. [39].

In Sec. 5.3 the amplitude stability for a few transversal modes was addressed. This analysis is not complete and needs extension to the other modes using Fourier transform techniques. We are working on this problem at present.

The spatial localization of the fastest-growing perturbation described by the maximum exponent is a very general result. It is also found for particle systems interacting *via* soft potentials [9], although the details of the power-law dependence of the localization measure $C_{1,\Theta}$ depend sensitively on the interaction potential. Also continuous systems in nonequilibrium stationary states exhibiting Rayleigh-Bénard convection have this localization property [40]. There it is found that the localized active zones contributing most to the perturbation vector for large positive Lyapunov exponents are involved in the creation and annihilation of defects of the roll pattern, resulting in the breaking or reconnection of Rayleigh-Bénard rolls [40].

Acknowledgements

We enjoyed many useful discussions with Predrag Cvitanović, Christoph Delgado, Astrid de Wijn, Bob Dorfman, Jean-Pierre Eckmann, Denis Evans, Rainer Klages, Joel Lebowitz, Ljubomir Milanović, Gary Morriss, David Mukamel, Günter Radons, David Ruelle, Ya. G. Sinai, Tooru Taniguchi, Walter Thirring, Henk van Beijeren, Jürgen Vollmer, Emmanuel Zabey, and participants of the workshop *Microscopic Chaos and Transport in Many-Particle Systems*, August 2002, in Dresden. We gratefully acknowledge access to the high-performance computing facility “Schrödinger” of the University of Vienna and support by the Austrian Fonds zur Förderung der wissenschaftlichen Forschung, Grants P11428-PHY and P15348-PHY.

References

- [1] H. A. Posch and W. G. Hoover, *Phys. Rev. A* **38**, 473 (1988).
- [2] H. A. Posch and W. G. Hoover, *Phys. Rev. A* **39**, 2175 (1989).
- [3] Wm. G. Hoover, *Time Reversibility, Computer Simulation, and Chaos*, (World Scientific, Singapore, 1999).
- [4] D. J. Evans and G. P. Morriss, *Statistical mechanics of nonequilibrium liquids*, Academic Press, London, 1990.
- [5] P. Gaspard, *Chaos, Scattering, and Statistical Mechanics*, (Cambridge University Press, 1998).
- [6] J. R. Dorfman, *An Introduction to Chaos in Nonequilibrium Statistical Mechanics*, (Cambridge University Press, 1999).
- [7] H. A. Posch and R. Hirschl, “Simulation of Billiards and of Hard-Body Fluids”, p. 269 - 310, in *Hard Ball Systems and the Lorenz Gas*, edited by D. Szasz, Encyclopedia of the mathematical sciences **101**, Springer Verlag, Berlin (2000).

- [8] R. Hirschl, “Computer simulation of hard-disk and hard-sphere systems: Lyapunov modes and stochastic color conductivity”, Master’s thesis, University of Vienna, 1999.
- [9] H. A. Posch and Ch. Forster, “Lyapunov instability and collective tangent space dynamics of fluids”, Lecture Notes on Computer Science **2331**, *Computational Science - ICCS 2002*, vol. 3, p.1170, edited by P.M.A. Soot, C.J.K. Tan, J.J. Dongarra, and A.G. Hoekstra, Springer, Berlin, 2002.
- [10] Wm. G. Hoover, H. A. Posch, Ch. Forster, Ch. Dellago, and M. Zhou, J. Stat. Phys. **109**, 765 (2002).
- [11] Lj. Milanović, H.A. Posch, and Wm. G. Hoover, CHAOS **8**, 455 - 461 (1998).
- [12] Lj. Milanović, H.A. Posch, and Wm. G. Hoover, Molec. Phys., **95**, 281 - 287 (1998).
- [13] Lj. Milanović and H. A. Posch, J. Molec. Liquids, **96-97**, 221 - 244 (2002).
- [14] Lj. Milanović, “Dynamical instability of two-dimensional molecular fluids: hard dumbbells”, Ph.D. thesis, University of Vienna, 2001.
- [15] J. D. Bernal and S. V. King, in *Physics of Simple Liquids*, H. N. V. Temperley, J. S. Rowlinson, and G. S. Rushbrooke eds., page 231, (North-Holland, Amsterdam, 1968).
- [16] B. J. Alder and T. E. Wainwright, Sci. Am. **201**(4), 113 (1959).
- [17] T. Einwohner and B. J. Alder, J. Chem. Phys. **49**, 1458 (1968).
- [18] J.-P. Hansen and I. R. McDonald, *Theory of simple liquids*, (Academic Press, London, 1991).
- [19] T. M. Reed and K. E. Gubbins, *Applied Statistical Mechanics*, (McGraw Hill, Tokyo, 1973).
- [20] J.-P. Eckmann and O. Gat, J. Stat. Phys. **98**, 775 (2000).
- [21] J.-P. Eckmann and E. Zabey, private communication, and *International Workshop and Seminar on Microscopic Chaos and Transport in Many-Particle Systems*, (Max Planck-Institut für Physik komplexer Systeme, Dresden, 2002), unpublished.
- [22] S. McNamara and M. Mareschal, Phys. Rev. E **64**, 051103 (2001).
- [23] M. Mareschal and S. McNamara, *International Workshop and Seminar on Microscopic Chaos and Transport in Many-Particle Systems*, (Max Planck-Institut für Physik komplexer Systeme, Dresden, 2002), this issue.
- [24] A. de Wijn and H. van Beijeren, private communication, and *International Workshop and Seminar on Microscopic Chaos and Transport in Many-Particle Systems*, (Max Planck-Institut für Physik komplexer Systeme, Dresden, 2002).
- [25] T. Taniguchi, C. P. Dettmann, and G. P. Morriss, J. Stat. Phys. **109**, 747 (2002).

- [26] T. Taniguchi and G. P. Morriss, Phys. Rev. E **65**, 056202 (2002).
- [27] Ch. Dellago, H.A. Posch, and Wm. G. Hoover, Phys. Rev. E **53**, 1485 (1996).
- [28] Wm. G. Hoover, K. Boercker, and H. A. Posch, Phys. Rev. E **57**, 3911 (1998).
- [29] V. I. Oseledec, Trans. Mosc. Math. Soc. **19**, 197 (1968).
- [30] J.-P. Eckmann and D. Ruelle, Rev. Mod. Phys. **57**, 617 (1985).
- [31] C. P. Dettmann and G. P. Morriss, Phys.Rev. E **53**, R5541 (1996).
- [32] D. Ruelle, J. Stat. Phys. **95**, 393 (1999).
- [33] D. J. Evans, E. G. D. Cohen, and G. P. Morriss, Phys. Rev. A **42**, 5990 (1990).
- [34] G. Benettin, L. Galgani, A. Giorgilli, and J. M. Strelcyn, Meccanica **15**, 9 (1980).
- [35] I. Shimada and T. Nagashima, Proc. Theor. Phys. **61**, 1605 (1979).
- [36] Ch. Forster and H. A. Posch, unpublished.
- [37] Ch. Forster, “Lyapunov instability of two-dimensional fluids”, Master’s Thesis, University of Vienna, 2002.
- [38] T. Taniguchi and G. P. Morriss, preprint.
- [39] Ch. Dellago, Wm. G. Hoover, and H. A. Posch, Phys. Rev. E **65**, 056216 (2002).
- [40] D. A. Egolf, I. V. Melnikov, W. Pesch, and R. E. Ecke, Nature **404**, 733 (2000).